ADVANCED ENERGY MATERIALS
www.advenergymat.de

Interplay of Optical, Morphological, and Electronic Effects of ZnO Optical Spacers in Highly Efficient Polymer Solar Cells

Sadok Ben Dkhil, David Duché, Meriem Gaceur, Anil K. Thakur, Fatima Bencheikh Aboura, Ludovic Escoubas, Jean-Jacques Simon, Antonio Guerrero, Juan Bisquert, Germà Garcia-Belmonte, Qinye Bao, Mats Fahlman, Christine Videlot-Ackermann, Olivier Margeat, and Jörg Ackermann**

Optical spacers based on metal oxide layers have been intensively studied in poly(3-hexylthiophene) (P3HT) based polymer solar cells for optimizing light distribution inside the device, but to date, the potential of such a metal oxide spacer to improve the electronic performance of the polymer solar cells simultaneously has not yet be investigated. Here, a detailed study of performance improvement in high efficient polymer solar cells by insertion of solution-processed ZnO optical spacer using ethanolamine surface modification is reported. Insertion of the modified ZnO optical spacer strongly improves the performance of polymer solar cells even in the absence of an increase in light absorption. The electric improvements of the device are related to improved electron extraction, reduced contact barrier, and reduced recombination at the cathode. Importantly, it is shown for the first time that the morphology of optical spacer layer is a crucial parameter to obtain highly efficient solar cells in normal device structures. By optimizing optical spacer effects, contact resistance, and morphology of ZnO optical spacers, poly[[4,8-bis[(2-ethylhexyl)oxy]benzo[1,2-b:4,5-b′]dithiophene-2,6diyl] [3-fluoro-2-[(2-ethylhexyl)carbonyl] thieno[3,4-b]thiophenediyl]] (PTB7):[6,6]-phenyl-C71-butyric acid ($PC_{70}BM$) bulk heterojunction solar cells with conversion efficiency of 7.6% are obtained in normal device structures with all-solution-processed interlayers.

1. Introduction

Polymer solar cells are nowadays one of the most relevant approaches for future low cost solar cells as they combine low cost processing from solution and high efficiency. Indeed power conversion could be increased beyond 10% efficiency due to intense research in new low band gap polymers absorbing more light in the visible.[1,2] While the optoelectronic properties of the photoactive layer determine the theoretically maximum photocurrent generation and thus the efficiency of the solar cell, interfacial layers sandwiching the photoactive layer are of equal importance as they have to provide efficient charge carrier extraction towards the electrodes avoiding hereby losses such as non-Ohmic contact, charge carrier recombination and exciton quenching at the interfaces.[3,4] Amongst solution processed interfacial materials, metal oxides such as zinc oxide (ZnO),[5–11] titanium dioxide (TiO_2)[12–14] or hybrid reduced graphene oxide (RGO)/metal oxide nanocomposite using either ZnO or TiO_2[15] are very promising candidates due to their suitable energy level for electron extraction from fullerene derivatives, together with simple synthesis and good environmental compatibility in terms of toxicity and energy impact. To further reduce the energy barrier between the cathode and an active layer, interfacial dipole layers can be applied via surface modification onto metal oxide interlayers.[11,16] Surface modification of ZnO interlayers with ethanolamine lead to highly

Dr. S. Ben Dkhil, Dr. M. Gaceur, Dr. A. K. Thakur,
Dr. C. Videlot-Ackermann, Dr. O. Margeat, Dr. J. Ackermann
Aix Marseille Université
CNRS, CINaM UMR 7325, 13288, Marseille, France
E-mail: ackermann@cinam.univ-mrs.fr
Dr. D. Duché, F. B. Aboura, Prof. L. Escoubas, Dr. J.-J. Simon
Aix Marseille Université, CNRS, Université de Toulon
IM2NP UMR 7334, 13397, Marseille, France
E-mail: jean-jacques.simon@univ-amu.fr
Dr. A. Guerrero, Prof. J. Bisquert, Prof. G. Garcia-Belmonte
Photovoltaics and Optoelectronic Devices Group
Departament de Física
Universitat Jaume I
12071, Castelló, Spain
Prof. J. Bisquert
Department of Chemistry, Faculty of Science
King Abdulaziz University
Jeddah, Saudi Arabia
Dr. Q. Bao, Prof. M. Fahlman
Department of Physics, Chemistry and Biology
Linkoping University
58183, Linkoping, Sweden

DOI: 10.1002/aenm.201400805

efficient solar cells with fill factors up to 73% demonstrating that metal oxide materials can compete with best interfacial layers obtained by evaporation techniques.[11] Beside their electronic properties, such metal oxide layers introduce so called optical spacer (OSP) effects that modify the light distribution inside solar cells using regular device structures.[17–20] Indeed, optical spacers placed between the active layer and the cathode allow improving spatial distribution of light inside the multilayer stack of the solar cell and thus optimizing the absorption in the photoactive layer. While most of the work on OSP is based on poly 3-hexylthiophene (P3HT): [6,6]-phenyl-C61-butyric acid methyl ester ($PC_{60}BM$) solar cells, recently the efficiency of solution processed oligomer solar cells could be increased to 8.94% by using ZnO OSP layers demonstrating the general relevance of OSP for OPV.[21] Importantly, it could be shown in the case of oligomer solar cells, that ZnO OSP layers not only increase light absorption but also improve the electronic properties of the devices by reducing recombination at the electrode. However, although optical spacer have been intensively studied in polymer solar cells, to be best of our knowledge a detailed study of the electric properties introduced by OSP layer to polymer solar cells was so far not done. For example in the work of Janssen on ZnO based optical spacer, an additional interface layers of LiF were used to improve the cathode/polymer interface, that did not allow to observe the electronic improvement related to ZnO layers.[17] Furthermore, a deeper understanding of metal/ZnO contact,[15] electronic properties of ZnO layers and optical redistribution at the cathode seems crucial to optimize the performance of polymer solar cells using metal oxide OSP layers. The high potential of ZnO OSP layers to improve solar energy efficiency in OPV has motivated us to study in detail the complex interplay of electronic, morphological and optical spacer effects of ZnO OSP layers in polymer solar cells.

In this scenario, we combined optical modeling, UV–vis absorption spectroscopy, current–voltage analysis, external and internal quantum efficiency, transient open circuit voltage decay, impedance measurements and atomic force microscopy analysis to investigate ZnO OSP layers in polymer solar cells. Different features lead us to choose two model systems P3HT:$PC_{60}BM$ and poly[[4,8-bis[(2-ethylhexyl)oxy]benzo[1,2-b:4,5-b′]dithiophene-2,6diyl] [3-fluoro-2-[(2-ethylhexyl)carbonyl] thieno[3,4-b]thiophenediyl]] (PTB7):[6,6]-phenyl-C71-butyric acid ($PC_{70}BM$), respectively. First, P3HT:$PC_{60}BM$ solar cells have been intensively studied in both normal and inverted device structures.[5–14] Furthermore P3HT:$PC_{60}BM$ blends can be processed into thick layers with high efficiencies. This allows reducing interference effects inside the cells that makes a detailed study of the electronic properties of ZnO OSP layers more accessible.[17] Moreover, the optical properties of ZnO layers in P3HT: $PC_{60}BM$ based solar cell have been studied in details making them a good model system of optical spacers.[15] We further chose PTB7:$PC_{70}BM$ blends as a new model system for highly efficient low band polymer solar cells as it has been intensively studied recently[22–24] and successfully combined with ZnO interfacial layers.[15] Highly efficient PTB7:$PC_{70}BM$ devices have been obtained with thin layers around 80–90 nm thickness, which make PTB7 based devices very sensible to optical spacer effects and necessitates a combined approach of optical and electronic investigations to better understand the Al/ZnO interface. Our device structure using active layers based on P3HT:$PC_{60}BM$ and PTB7:$PC_{70}BM$, respectively, is shown in **Figure 1**.

In this work, we report the preparation of a cluster-free ZnO nanoparticle solution in isopropanol by using ethanolamine (EA) as surfactant. This allows processing of ZnO optical spacers on top of the photoactive layer with improved film morphology and surface roughness compared to untreated ZnO. By the comparison of P3HT:PCBM devices using optical spacers based on EA modified ZnO as well as untreated ZnO with bare Al contact, we found that only in the first case, all parameters determining the performance of the solar cells, i.e., short-circuit current density, fill factor and open-circuit voltage, are strongly improved by the inclusion of the OSP layer. Importantly, an increase in short circuit occurs here without an increase in the total light absorption inside the active layer and is only related to improved charge carrier lifetime and electron extraction at the cathode. In the case of untreated ZnO leading to interlayers of increased surface roughness, we found only intermediate improvement in device performance, mainly due to strong losses in fill factor. Thus changes in electric improvement of the solar cells could be correlated to the changes in layer morphology of the optical spacers. Application of the different ZnO interlayers to PTB7:$PC_{70}BM$ solar cells confirms the role of OSP layer morphology to obtain high fill factor and thus high efficiency. To the best of our knowledge, this is the first time that the impact of OSP layer morphology on the device performance could be demonstrated. By optimizing optical, morphological and electronic properties of ZnO based OSP layers, we obtain PTB7:$PC_{70}BM$ solar cells with 7.6% using normal device with all solution processed interlayers.

2. Results and Discussions

2.1. ZnO Nanoparticle Solutions for OSP Processing

First, ZnO solutions were developed for solution processing of optical spacer on top of polymer blends. As isopropanol (IPA) is known not to dissolve P3HT:$PC_{60}BM$ blends,[25] ZnO nanoparticle dispersion in IPA were prepared by adding ethanolamine (EA) as dispersing agent leading to two ZnO solutions of different optical aspects as shown in Figure 1.[26] Dynamic light scattering (DLS) measurements reveal that ZnO nanoparticles without EA modification form aggregates in IPA of ≈30 nm in diameter, and thus much larger than the single particle size of 5 ± 1 nm in diameter as obtained from HR-TEM analysis. By adding EA as surfactant, the DLS value drops to 7 nm, which corresponds to hydrodynamic diameter of the nanoparticles. Importantly ultrasonic treatment was needed to gradually reduce the cluster size after EA treatment and has to be performed at least during 30 min to obtain a cluster free solution of isolated ZnO nanoparticles. In the following, EA modified ZnO is denoted as ZnO_{EA}, while untreated ZnO is signed as ZnO. Remarkably, ZnO_{EA} nanoparticles in IPA form highly stable cluster free solution up to a concentration of 30 mg/ml over several days (Figure S1, Supporting Information). In order to evaluate the impact of EA modification on the

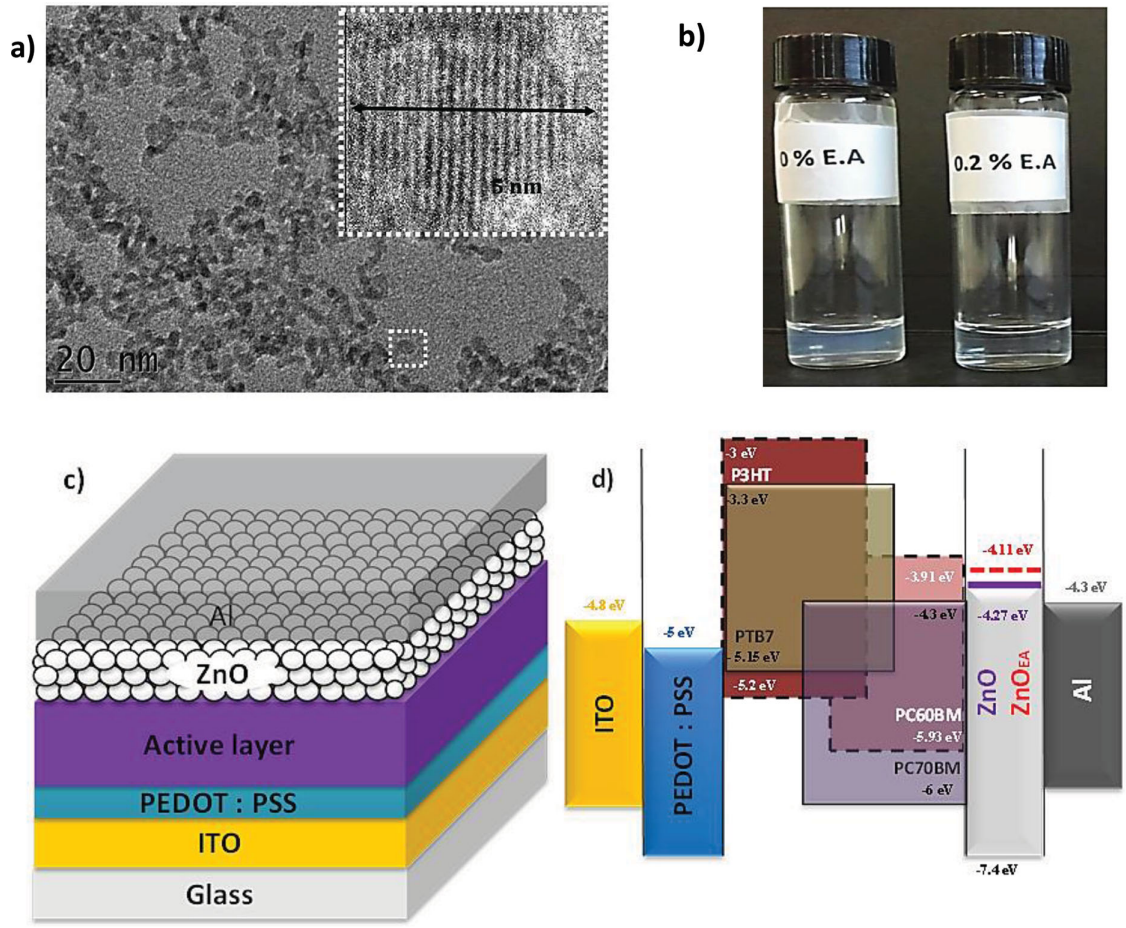

Figure 1. a) TEM image and HR-TEM of as synthesized ZnO nanoparticles, b) photograph of ZnO solutions in isopropanol as prepared and after EA modification, c) device structure, and d) energy level diagram of the solar cell using EA modified ZnO interfacial layers.

opto-electronic properties of ZnO nanoparticles, we performed absorption and fluorescence spectra of ZnO nanoparticles with and without EA modification in solution and spin coated on glass substrates as shown in **Figure 2**a,b, respectively. Obviously, grafting of EA on the surface of ZnO does not alter the absorption of ZnO leading to highly transparent films in the visible, while a strong UV absorption with an absorption onset at 360 nm is observed, which characterizes the absorption of 5 nm sized ZnO nanoparticles. The fluorescence spectra in Figure 2b show the impact of EA on the emission of ZnO layers with or without EA modifications. It can be seen that the intensity of the defect emission band of ZnO_{EA} centered at 450 nm is not affected by the adding of EA in both solution and in thin film. This is in contrast to recent work on ZnO interlayers for inverted polymer solar cells, in which poly(ethylene oxide) modification to the nanoparticle surface reduces strongly the intensity of defect emission due to efficient passivation of surface traps.[27] Therefore we conclude that EA is not interacting with defect states at the surface of ZnO nanoparticles. Looking more deeply into the possible modifications to the surface electronic structure induced by the EA, XPS and UPS measurements of films from both ZnO and ZnO_{EA} were carried out. The XPS did not indicate any significant changes in the O 1s and Zn 2p core levels upon EA treatment. In Figure 2c (left panel) the UPS-derived work function of the two types of films is shown. The EA treatment is found to decrease the work function from 4.27 eV to 4.11 eV, which can be assigned to dipolar polarization of the ZnO surface via the adsorption of EA.[11] The edge of the frontier peak in the occupied electronic structure also is modified, from 3.95 eV to 4.06 eV, which together with the work function shift suggests a near constant position of the valence band edge vs the vacuum level. The down shift in work function for the ZnO_{EA} is of significance to $PC_{60}BM$ based solar cells, as the so-called negative pinning energy of $PC_{60}BM$ can vary between 4.1 to 4.4 eV depending on batch and environmental exposure.[28–30] As a consequence, ZnO_{EA} films are expected to form pinned contacts with $PC_{60}BM$, whereas for the higher work function ZnO films, there may be a barrier of up to ≈0.1 eV with a corresponding loss in V_{OC} for those cases. Hence, ZnO_{EA} compared to bare ZnO nanoparticles should allow more efficient extraction of electrons towards the cathode while still blocking hole diffusion, as the valence band edge is situated deeper vs the Fermi level and constant vs the vacuum level after EA-treatment. Improved charge extraction can be expected in the case of $PC_{70}BM$ as acceptor due to reduced contact resistance as observed in inverted solar cells using EA modified ripple-structure ZnO extraction layer.[11]

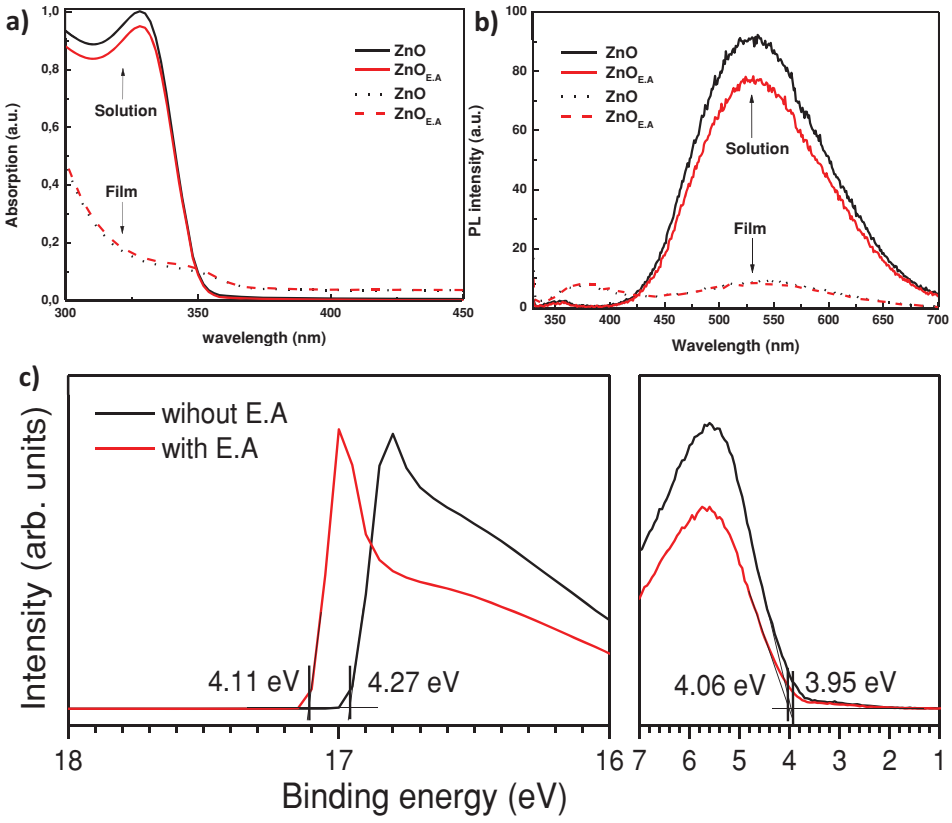

Figure 2. a) Absorption and b) fluorescence spectra of ZnO nanoparticles with and without EA modification in isopropanol as well as spin coated on glass substrates. c) XPS/UPS spectra of ZnO nanoparticles with and without EA modification.

2.2. ZnO Optical Spacers Studied in P3HT:$PC_{60}BM$ Solar Cells Using Thick Active Layers

In order to focus on the electronic changes of polymer solar cells due to the intercalation of ZnO OSP layers between the cathode and the polymer blend, we aimed first to reduce optical interference effects inside the solar cells and studied therefore P3HT:$PC_{60}BM$ solar cells using thick active layers. To study the light distributions inside the polymer solar cells in detail, we used a transfer matrix method (TMM) as an elegant method to simulate the optical properties of interferential thin films systems.[31,32] **Figure 3**a shows the number of absorbed photons inside the active layer as a function of the P3HT:$PC_{60}BM$ layer thickness for different ZnO layer thicknesses. For solar cells using thin P3HT:$PC_{60}BM$ layers, we find a strong variation of number of absorbed photons up to 35% when the ZnO layer thickness is varying from 0 to 70 nm, which is in accordance with work of Janssen et co-worker published recently.[17] In the case of P3HT:$PC_{60}BM$ layers of 200 nm thickness, maximal 8% variation in photon absorption inside the active layer is induced by using ZnO layer from 0% up to 70 nm making a focus on the electronic changes of the device due to the introduction of the ZnO layer more accessible. We consider first solar cells using 200 nm active layer of P3HT:$PC_{60}BM$ in combination with a 30 nm thick ZnO layer. In this particular case, the number of absorbed photons inside the active layer was calculated to be almost constant compared to solar cells without ZnO layers (Figure 3a). As ligand modification of ZnO surfaces with EA should have an impact on the electronic properties of the ZnO nanoparticles and thus on the interfacial properties, we further compared ZnO_{EA} layers with untreated ZnO layers. Figure 3b shows the corresponding current density-voltage (J–V) curves of three representative devices under simulated AM1.5 illumination revealing that all photovoltaic parameters including short circuit current density (J_{sc}), open circuit voltage (V_{OC}), fill factor (FF) and power conversion efficiency (PCE) of the P3HT:$PC_{60}BM$ solar cells are improved by the intercalation of ZnO_{EA}. The ZnO_{EA} improves J_{sc} from J_{sc} = 6.18 mA cm^{-2} to 7.20 mA cm^{-2}, V_{oc} from 0.49 V to 0.58 V and fill factor FF from 50% to 65% leading to an overall efficiency improvement from 1.53% to 2.75%. As the optical calculations indicate that the number of absorbed photons was not modified inside the active layer, the increase in J_{sc} by 17% can be addressed to a pure electrical effect. When regarding untreated ZnO OSP layers, we observe only intermediate values of performance improvement. While V_{OC} and J_{SC} were similarly improved compared to ZnO_{EA}, FF was even decreased compared to the reference cell although the thickness of both ZnO layers was identical indicating that EA introduces additional parameters to the ZnO solutions to enhance the performance of the solar cells. The analysis of serial and shunt resistance of the three solar cells reveals two changes related to the intercalation of ZnO between the polymer blend and the Al cathode. First of all, shunt resistance is clearly

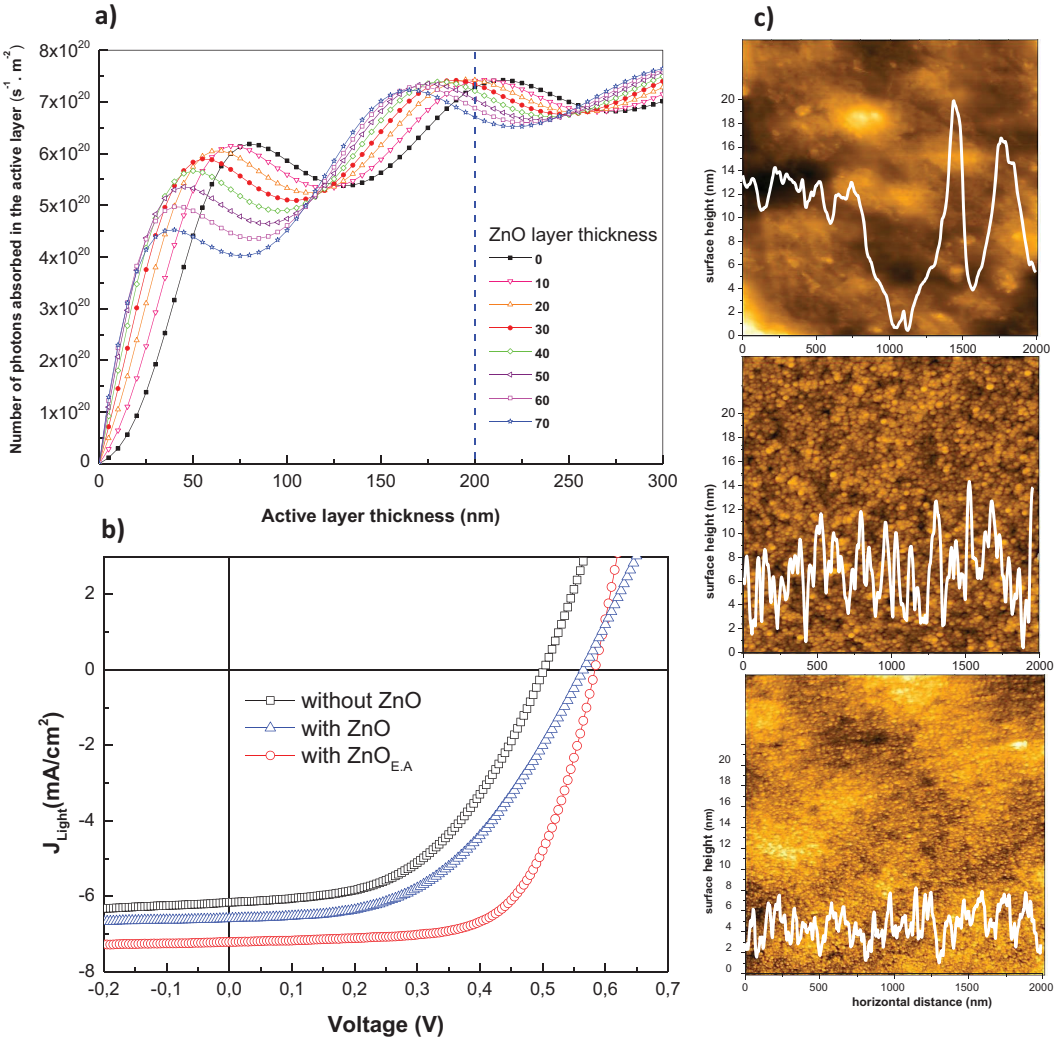

Figure 3. a) Number of photons absorbed inside a P3HT: $PC_{60}BM$ layer as a function of P3HT: $PC_{60}BM$ layer thickness calculated for different ZnO layer thicknesses. b) *J–V* curves under illumination of P3HT:$PC_{60}BM$ cells using only bare contacts, ZnO and ZnO_{EA} as interfacial layers. c) AFM images (2×2 μm^2) and surface profiles of bare P3HT: $PC_{60}BM$ layers (top), covered with a ZnO (midle) and with a ZnO_{EA} layers (bottom); ZnO and ZnO_{EA} layers have identical average thickness of 30 nm.

improved from $R_{sh} = 1.19\ 10^3\ \Omega\ cm^2$ to $R_{sh} = 3.1\ 10^3\ \Omega\ cm^2$ by applying an OSP layer based on ZnO_{EA}. This can be addressed to the hole blocking behavior of ZnO by that reducing leakage current at the cathode related to recombination of hole and electrode at the Al interface. We also observe a reduction in serial resistance from $R_s = 12.27\ \Omega\ cm^2$ to $R_s = 5.69\ \Omega\ cm^2$ for ZnO_{EA} layers compared to the reference cell (**Table 1**). Interestingly in the case of untreated ZnO, shunt resistance R_{sh} is only slighty increase to $R_{sh} = 1.3\ 10^3\ \Omega\ cm^2$ and, more importantly, R_s is even increased to $R_s = 24{,}1\ \Omega\ cm^2$ being the origin of the poor fill factor of solar cells using untreated ZnO OSP layers. The difference in R_s can be partly understood by taking into account the UPS/XPS results indicating a down shift of the work function upon adding of EA. This improves charge carrier extraction for ZnO_{EA} layers and contributes to a total reduction of the R_s.[11] In order to study the effect of EA further, we analyzed layer morphology of bare P3HT:$PC_{60}BM$ layers and those covered with ZnO and ZnO_{EA}, respectively, by Atomic force microscopy (AFM). As it can be seen in Figure 3c, ZnO_{EA} layers are homogenous, closely packed and very smooth, while untreated ZnO lead to layers containing nanoparticle agglomerates and high surface roughness as indicated by calculated mean surface roughness. ZnO_{EA} layers improve the surface roughness of bare P3HT:$PC_{60}BM$ layers from an initial RMS value of 9.1 nm to a value of 2.7 nm. Additionally, low peak-to-peak variation in the same range as the size of the ZnO nanoparticles of 4 nm are observed (insets of Figure 3b) leading to a planarization of the interface region. In contrast, unmodified ZnO lead to an intermediate RMS value of 4.8 nm as well as peak to peak variations up to 12 nm corresponding almost to half of the layer thickness. However, we could not observe holes inside untreated ZnO layers by AFM analysis. This is in accordance with the fact that both ZnO layers lead to solar cells with almost identical V_{oc} values pointing towards a negligible amount of short circuits due to potential holes inside the ZnO layer. Recent work by Liang

Table 1. Photovoltaic parameters of P3HT:$PC_{60}BM$ and PTB7:$PC_{70}BM$ solar cells using untreated ZnO and ZnO_{EA} interfacial layers. P3HT:$PC_{60}BM$ and PTB7:$PC_{70}BM$ cells using a bare Al contact are shown as reference. Photovoltaic parameters are given for best devices, while average PCEs are obtained standard deviation calculations for 9 devices.

	d [nm]	V_{oc} [V]	RMS [nm]	J_{sc} [mA cm^{-2}]	FF [%]	PCE [%]	R_s [Ω cm^2]	R_{sh} [Ω cm^2]	Average PCE (± std. dev.)
no ZnO	0	0.49	9.1	6.2	50	1.5	12.3	1190	(1.40 ± 0.13)
ZnO	30	0.56	4.7	6.6	49	1.8	24.1	1300	(1.72 ± 0.06)
ZnO_{EA}	30	0.58	2.7	7.2	65	2.8	5.7	3166	(2.70 ± 0.08)
Vacuum-annealed P3HT:$PC_{60}BM$ layer									
no ZnO	0	0.53	8.5	7.1	55	2.1	8.3	2000	(1.85 ± 0.21)
ZnO_{EA}	30	0.56	2.8	9.5	65	3.5	4.9	2941	(3.42 ± 0.07)
Vacuum-annealed PTB7:$PC_{70}BM$ layer									
no ZnO	0	0.68	1.4	14.3	59	5.8	6.8	1025	(5.22 ± 0.41)
ZnO	20	0.73	3.1	14.6	62	6.6	6.6	1060	(6.36 ± 0.18)
ZnO_{EA}	20	0.75	1.9	15.5	66	7.6	5.3	1700	(7.51 ± 0.08)

et al. on the role of ZnO buffer in inverted solar cells indicated that the surface roughness of the ZnO layers is the dominant factor impacting strongly the devices performance.[9] It seems therefore reasonable to correlate the differences in serial resistance with changes in morphology of the ZnO layer. However, at this stage we cannot exclude that variation in fill factor is dominated by the reduction of the extraction barrier between ZnO and $PC_{60}BM$ due to EA treatment of ZnO. Therefore we further performed devices using ZnO_{EA} solution, but with still existing NP clusters as only short sonication treatments were used. The corresponding AFM analysis show that the layers obtained with short sonicated ZnO_{EA} presents an intermediate morphology that contains of smaller aggregates of ZnO with a lower amount of areas with high peak to peak compared to untreated ZnO and former ZnO_{EA} with a still high with a RMS value of 4.3 nm (Figure S3, Supporting Information). The corresponding devices show an intermediate fill factor of 55%, which are clearly reduced compared to smooth ZnO_{EA} layer with fill factors of 64%. Thus, our results reveal that layer morphology plays an important role in the electric performance of the ZnO OSP layers. We can hypothesis that reasons for this improved charge extraction may be the more densely packed layers leading to improved contact to P3HT:$PC_{60}BM$ blend as proposed in the case of inverted device structures.[9] Furthermore it can be speculated that large thickness variations, which are present in the case of untreated ZnO layers, generate locally strong variation in electron density due to thickness dependence of the electric field at the interface. Thus, high charge carrier density may increase charge carrier recombination locally as well as increase resistivity by thermal heating.

2.3. Electronic Improvement of Polymer Solar Cells Using ZnO Based OSP Layers

In order to get a more deeper understanding of the physical processes of P3HT:$PC_{60}BM$ devices using ZnO_{EA} interfaces, we combined external quantum efficiency (EQE) measurements, optical simulations and reflection measurements of complete devices that allow to determine the internal quantum efficiency (IQE) of the solar cell. In order to validate our optical model based on a transfer matrix method, we first measured and calculated the total optical absorption $A(\lambda)$ of devices without and with a 30 nm thick ZnO_{EA} interlayer as shown in **Figure 4**a, while Figure S2 (Supporting Information) shows the calculated distribution of light absorption inside the solar cells. Importantly, we obtain a very good agreement between the experimental measurements and the simulations. Both data show that the overall light absorption inside the solar cell is not increased over the whole absorption spectrum and even reduced in the visible spectrum from 500–650 nm. Figure 4b shows the corresponding EQE of P3HT:$PC_{60}BM$ solar cells using ZnO interlayers revealing that the efficiency of photon to electron conversion is increased over the whole absorption spectrum by the intercalation of ZnO_{EA}. In order to study more in detail the photocurrent generation inside the device, we determined the internal quantum efficiency of the devices as shown in Figure 4c. It can be seen that IQE is increased over the whole spectral range when considering the cell with a ZnO_{EA} interlayer. Thus both EQE and IQE characteristics give clear proof that the total increase in photocurrent by 17% is only due to the electronic properties of the ZnO_{EA} layer and is not related to OSP effects.

In order to study the electronic improvement in device performance due to the intercalation of the OSP layer more in detail, impedance spectroscopy measurements for samples containing bare Al and ZnO_{EA}/Al as cathode were performed.[24] The solar cells were measured at 1 sun light illumination conditions, where the applied DC voltage (V_{app}) ranges from 0 V to 0.6 V and the frequency of the AC perturbation varies from 50 Hz to 500 kHz. Two impedance spectra compared at similar carrier densities of both devices are shown in **Figure 5**a. The response is similar to recent results, in which the following processes were observed simultaneously: transport of carriers, recombination and resistive processes related with the contacts.[33] In the high frequency region, we observe the response of the transport properties of the blend.[34] As expected for active layers spin coated under similar conditions the magnitude of this resistance is similar and will not be

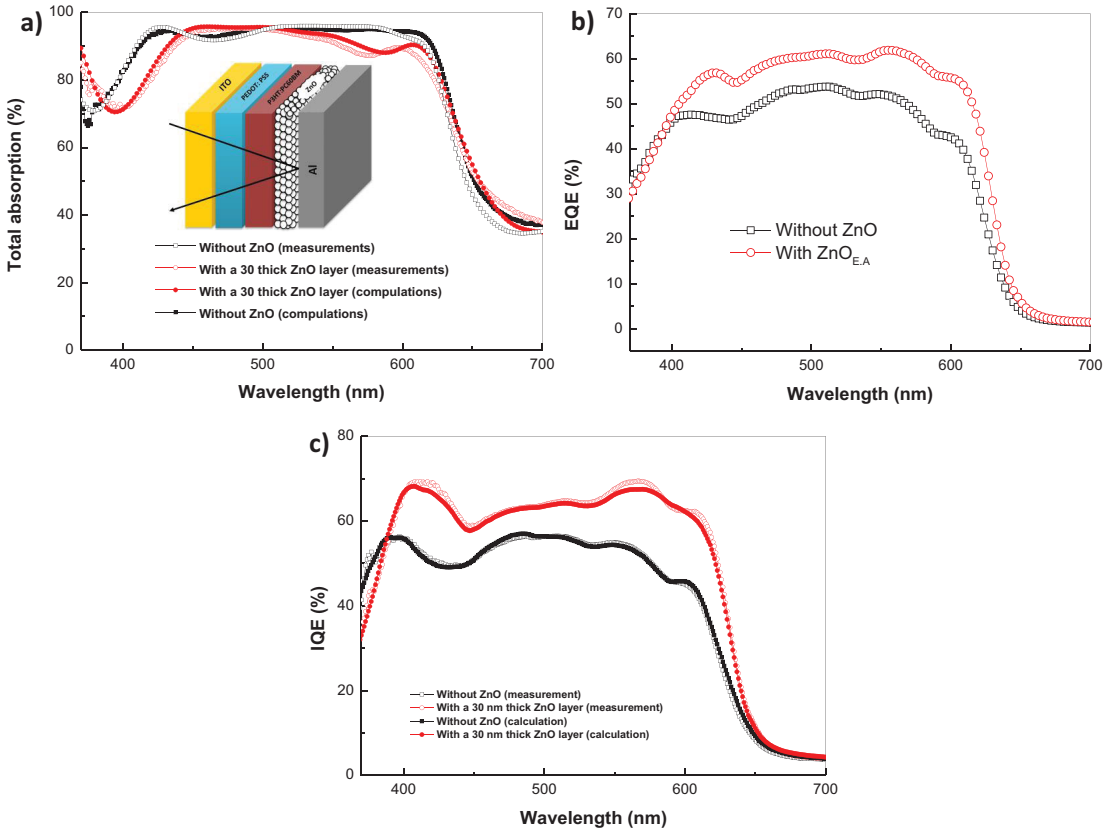

Figure 4. a) Experimental and simulated total absorption spectra, b) EQE spectra, and c) IQE spectra of the P3HT: $PC_{60}BM$ devices with or without a ZnO_{EA} interlayer.

further discussed here. Regarding the low frequency arc the response is dominated by the recombination processes and the interfaces of the active layer with the contacts. The device containing the interfacial layer ZnO_{EA}/Al shows only one arc in the Nyquist plot. This arc is related to the combination of recombination and charge accumulation of carriers within the active layer bulk. However, the device containing bare Al shows a small feature (contact resistance, R_{CO}) at frequencies below 300 Hz, which is better observed in the capacitance-frequency plot. Fitting results for the impedance spectroscopy measurements of the two devices are shown in Figure 5b. This contact resistance (R_{CO}) is related with the energy level mismatch between the active layer and the contact as previously published[33] and correlates well with the observed energy level pinning shown by UPS between ZnO_{EA} and fullerene. Only the sample containing bare Al contact shows this additional resistance (≈20 Ω cm^2). Importantly, this resistance contributes towards the series resistance of the device reducing the FF. On the other hand the sample containing ZnO_{EA} does not show any contact-related resistance indicating that energy levels of the active layer and cathode interface match and extraction of carriers at this contact. Additionally, the energy level mismatch at the active layer/Al interface can be addressed to a shift in the recombination resistance (Rrec), which contributes to the increase in V_{oc}.[35] We further performed transient open circuit voltage decay measurement (TOCVD)[36–38] of P3HT:$PC_{60}BM$ devices using or not ZnO_{EA} interfacial layers to study recombination kinetics and lifetime of photo-generated charge carriers. The lifetime τ of charge carriers in P3HT:$PC_{60}BM$ devices depending on the presence of a ZnO_{EA} interfacial layer is reported in Figure 5c. Two different regimes of τ as a function of V_{oc} can be observed. At high V_{oc}, the lifetime depends strongly on V_{oc} for both systems being consistent with bimolecular recombination mechanism where holes and electrons are mobile.[36,37] Recombination at the electrode mainly controls this V_{oc} regime, and since both structures use identical contact materials, ZnO_{EA} is expected to affect this recombination mechanism. Indeed, lifetime is clearly lifted up in this regime by the presence of ZnO_{EA}. At low V_{oc} values, lifetime has a small dependence on V_{oc} as this regime is governed by monomolecular recombination in which mobile charges recombine with trapped ones at the P3HT:$PC_{60}BM$ interface.[39] Here, we do not observe an effect of the ZnO_{EA} indicating the ZnO_{EA} only impact the cathode related interfaces as can be expected. Thus, the TOCVD analysis reveals that ZnO efficiently reduces charge carrier recombination at the cathode by blocking hole at the electrode. This interpretation fits well with the improvement of the shunt resistance in the devices using ZnO_{EA} OSP layer (Table 1) as well as the behavior of ZnO based OSP layers in oligomer solar cells.[21] However, it is worth to mention that interpretation of charge carrier recombination should

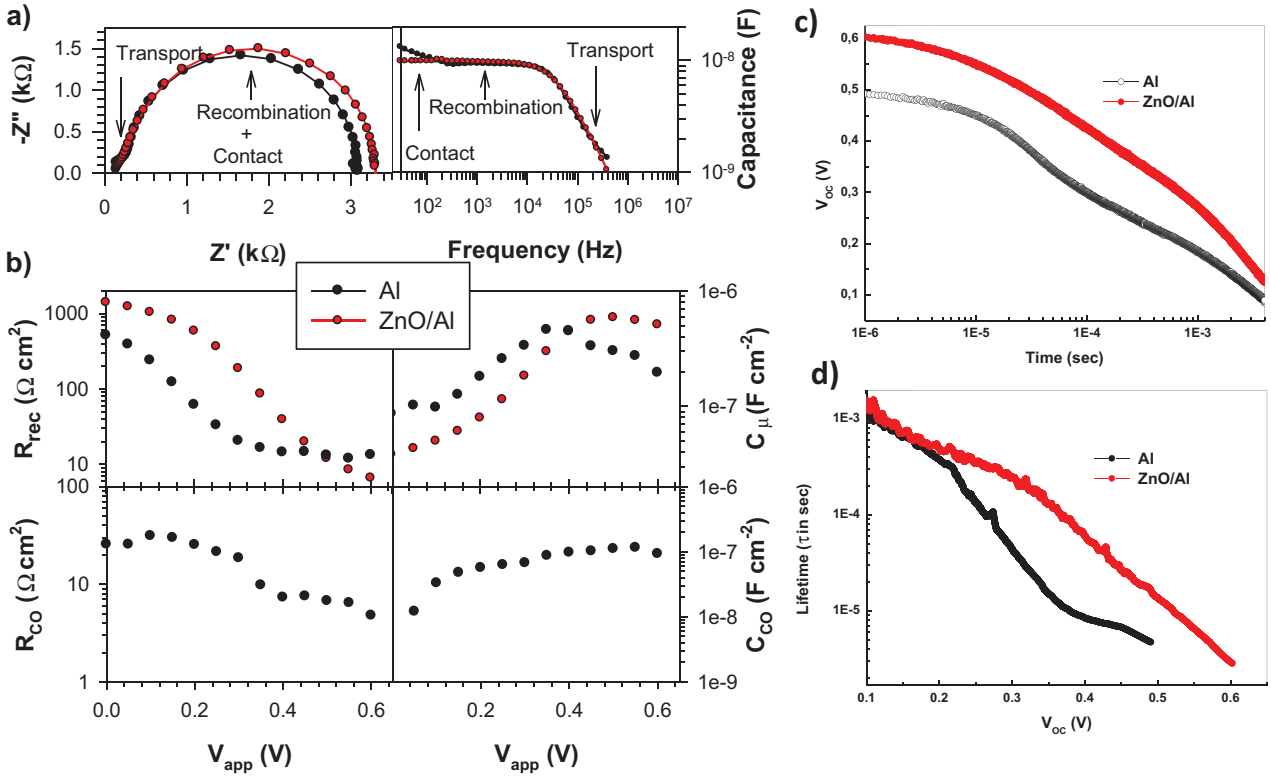

Figure 5. a) Nyquist and capacitance-frequency plots of P3HT: $PC_{60}BM$ solar cells containing either ZnO_{EA}/Al or bare Al cathode contact. Samples are compared at similar carrier densities at V_{app} = 0.3 and 0.1 V, respectively. b) Fitting results for IS measurements carried out in the DC in a). c) Transient open-circuit voltage decay measurements of devices with and without a ZnO_{EA} optical spacer layer.

be taken with caution. Charge carrier recombination mechanisms at the polymer blend/Al interface are complex and are also influenced by the change in contact resistance.[11] As observed in comparing recombination resistance in Figure 5b and transient lifetime in Figure 5c, a similar voltage shift occurs between devices with and without interlayer. This voltage shift of around 150 mV might be alternatively caused by the presence of a cathode dipole layer that changes the position of the electron energy levels and as a consequence reduces the contact barrier. In this case, the residual recombination would be determined by bulk processes instead of interfacial mechanisms.

After detailed study of electronic improvement related to the intercalation of a ZnO layer of 30 nm, we further optimize the P3HT:$PC_{60}BM$ devices. We find that device efficiency is gradually improved up to 30 nm, while further increase in ZnO_{EA} thickness lead to a reduction in performance mainly to loss in photocurrent (see Supporting Information Table S1) in accordance with the calculation in Figure 2. Importantly, the increase in ZnO layer thickness up to 70 nm kept fill factor and Rs almost constant. This result indicates clearly that the electronic properties of ZnO_{EA} layers up to 70 nm are not thickness limited, but controlled by the morphology of the interlayer. We further optimized the processing of the P3HT:$PC_{60}BM$ layers by using a drying step of the active layer in vacuum without thermal annealing.[40,41] The efficiency of the devices could be thereby further increased to 3.5% as shown in Table S1 and Figure S4 (Supporting Information).

2.4. PTB7:$PC_{70}BM$ Solar Cells Using ZnO OSP Layers

Our results on P3HT based solar cells highlighted the impact of OSP layer morphology on the electronic performance of the devices. In order to show the general relevance of this observation and especially for highly efficient low band gap polymer, we studied the light distribution in PTB7:$PC_{70}BM$ solar cells and corresponding device performance as a function of the ZnO layer included. In order to calculate the distribution of light absorption inside the solar cells, we first determined the optical indices of PTB7:$PC_{70}BM$ layers by ellipsometry analysis (see Supporting Information). Supporting Information Figure S5 show the measured and calculated ellipsometric angles Ψ and Δ for PTB7:$PC_{70}BM$ layers at five incident angles. The results shows excellent agreement between the measurements and the calculation. Figure S6 show the corresponding transmission-absorption-reflection (a) as well as calculated n and k spectra (b) that were then used as input in the TMM calculations. We calculated the number of photons absorbed inside the PTB7:$PC_{70}BM$ layer as a function of PTB7:$PC_{70}BM$ (0–300 nm) and ZnO_{EA} layer (0–70 nm) thicknesses as shown in **Figure 6**a. Without a OSP layer, there is an absorption maximum for a PTB7:PCBM layer at 220 nm thickness and second maximum with lower absorption at 90 nm. The second maximum corresponds to the optimal thickness found for highly efficient PTB7:$PC_{70}BM$ solar cells.[22–24] By considering layers thinner than 100 nm, we can see that the use of ZnO OSP layer is detrimental to the

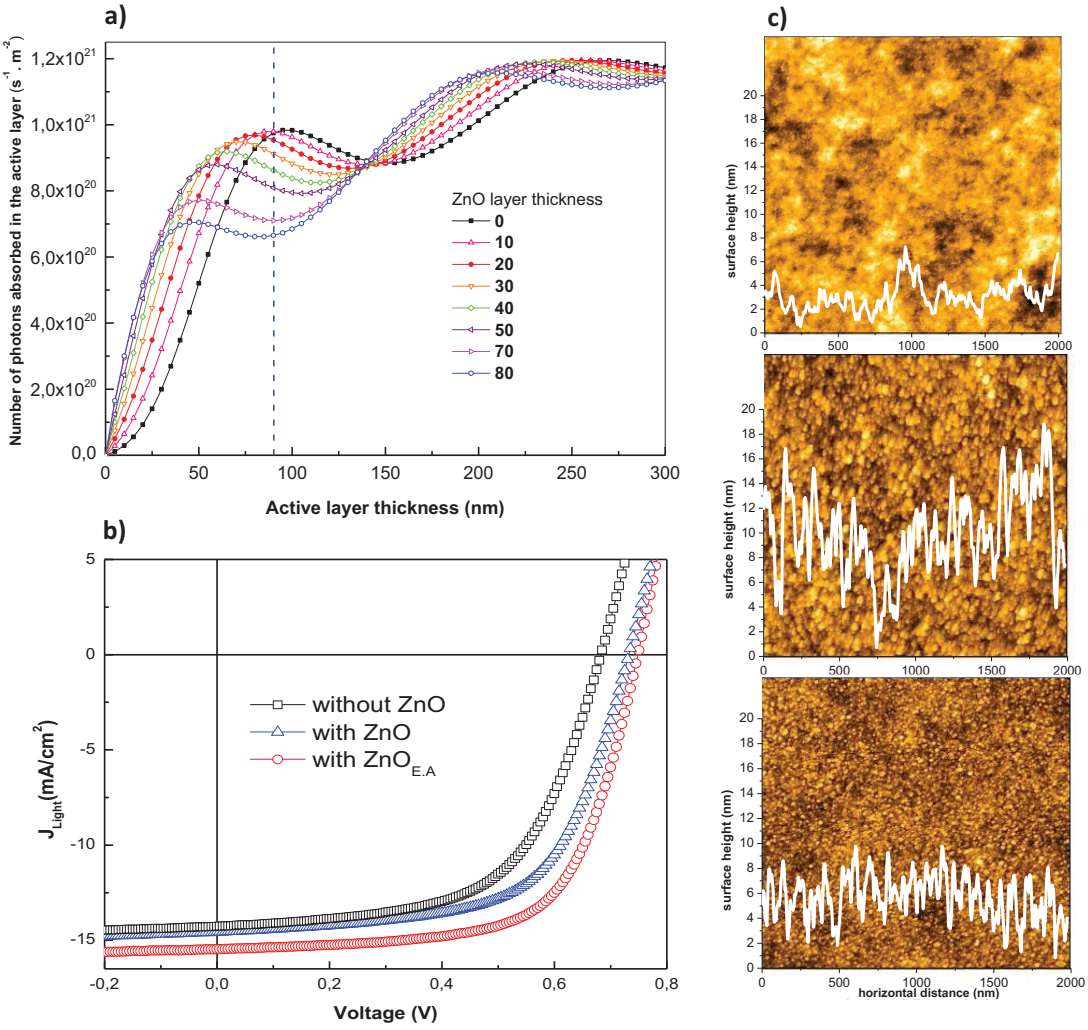

Figure 6. a) Number of photons absorbed inside a PTB7:$PC_{70}BM$ layer as a function of PTB7:$PC_{70}BM$ layer thickness calculated for different ZnO layer thicknesses, b) *J–V* curves under illumination of PTB7:$PC_{70}BM$ cells using only bar contacts or ZnO_{EA} as interfacial layer, c) AFM images (2×2 μm^2) and surface profiles of bare PTB7: $PC_{70}BM$ layers, covered with a ZnO and a ZnO_{EA} interlayers, respectively; all ZnO layers have identical average thickness of 20 nm.

device performance. The insertion of ZnO layers reduces the number of absorbed photons inside the PTB7:$PC_{70}BM$ blends constantly with increasing thickness. We can therefore expect that the thinnest ZnO layer should lead to highest photocurrent. As the electrical properties of ZnO layer depend on the layer morphology, a compromise between beneficial electronic effects related to morphology and negative OSP effects has to be found to optimize device performance. The experimental results of solar cells using different thicknesses of ZnO_{EA} layers are summarized in Supporting Information Table S1. It can be clearly seen that the thinnest ZnO layers generate the highest performance, while for thicker layers the photocurrent strongly decreased as expected.

In order to study the impact of the ZnO layer morphology on the device performance, we compared, as already done for P3HT:PCBM cells, PTB7:$PC_{70}BM$ devices using layers of untreated ZnO, ZnO_{EA} layers as well as bare Al contacts. Figure 6 and Table 1 show clearly that the use of ZnO_{EA} layers increases strongly the conversion efficiency from 5.8% for bare Al contact to 7.6%, while untreated ZnO layers result only in intermediate efficiency. Corresponding AFM analysis, shown in Figure 6c, reveal that ZnO_{EA} layers show strongly improved layer morphology with a RMS value of 1.8 nm, while untreated ZnO has a RMS of 3 nm and large aggregates of ZnO nanoparticles. Additionally, both R_h and R_s, are clearly improved for devices using ZnO_{EA} layers compared to untreated ZnO layers due to reduced contact barrier and improved morphology leading to higher fill factor and photocurrent. **Figure 7**a shows spectra of the total light absorption of inside the PTB7:$PC_{70}BM$ solar cells with and without ZnO_{EA} OSP layer. It can be seen that the overall light absorption is not increased over the whole absorption spectrum, but reduced below 600 nm, mostly in the UV spectrum from 380–450 nm. When regarding EQE and IQE spectra of PTB7 devices using optimized ZnO_{EA} layers and bare Al contacts, respectively, it can be clearly seen that the efficiency of photon

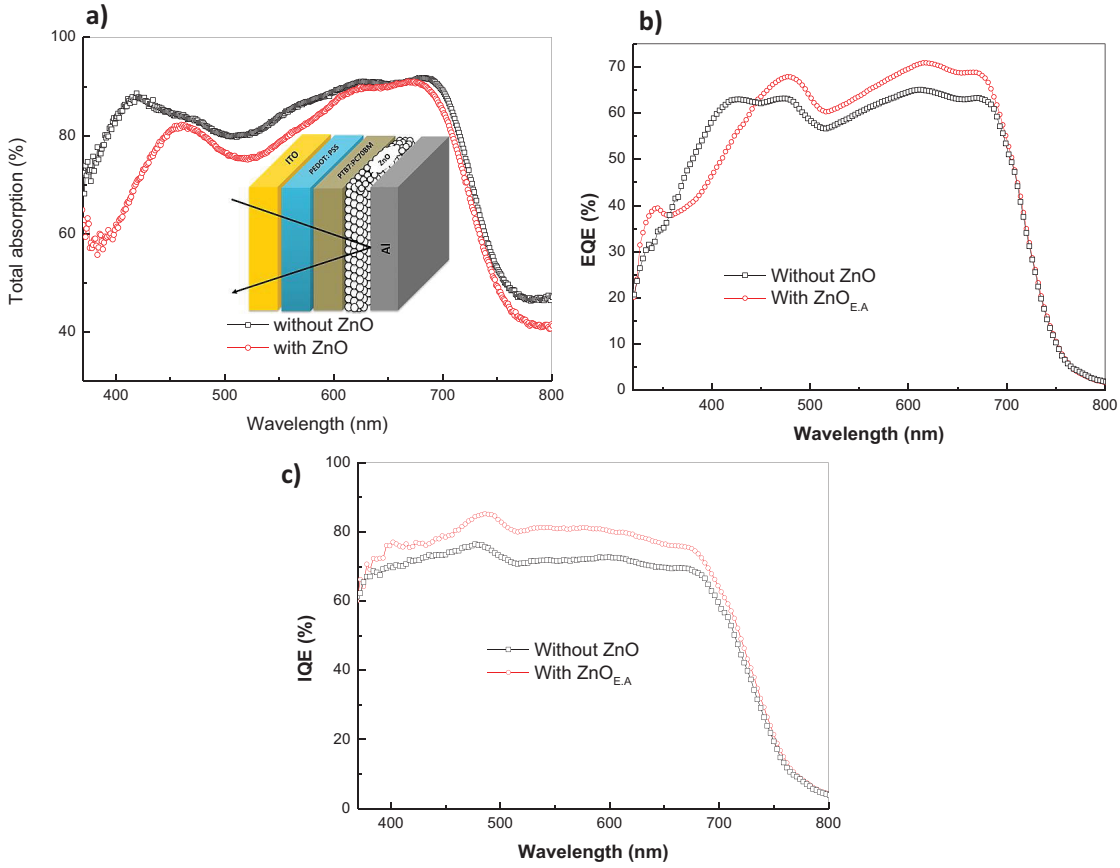

Figure 7. a) Total absorption spectra, b) EQE, and c) IQE spectra of PTB7:$PC_{70}BM$ solar cells with or without ZnO_{EA} interlayer.

to electron conversion is increased over the whole absorption spectrum by the intercalation of ZnO_{EA}. There are some EQE losses in the region below 450 nm as already observed in the case of oligomer based solar cells.[21] Here, we can address this effect clearly to the change in absorption inside the polymer blends as shown in Figure 7. The IQE spectrum of the device using a ZnO_{EA} layer is similar to that obtained for inverted solar cells using EA modification, while the IQE maximum of 85% at 486 nm fits well with an overall photocurrent I_{sc} of 15.5 mA cm^{-2}.[11] From our calculation of light distribution inside the PTB7:$PC_{70}BM$ layer, it can be seen that light absorption and thus photocurrent density inside the solar cells can be further increased by combining ZnO OSPs with thicker active layers. Therefore the use of OSP layer seems a promissing approach allowing to increase conversion efficiency. As ZnO_{EA} nanoparticle based OSP layers with thicknesses up to 70 nm are not limiting the charge transport of the cells, such relatively thick OSP layer would allow absorbing about 20% more photons inside a PTB7:$PC_{70}BM$ blend of by reducing optimal layer thickness from 254 nm down to 205 nm. This reduction of 20% in thickness for almost identical light absorption may be relevant. Indeed Foster et al. have shown very recently, that increasing the thickness of PTB7:$PC_{70}BM$ blends reduce strongly fill factor and thus device performance mainly due to poor electron transport inside the blend.[44] Thus improving connectivity in the fullerene phase in the PTB7:PCBM blends in combining OSP layers is a promising route towards further increase in efficiency of solar cells using normal device structures and PTB7 as donor polymer.

3. Conclusion

In this work, we combine optical modeling and experimental investigations to better understand ZnO OSP layers in polymer solar cells. We could demonstrate that insertion of a ZnO OSP improves strongly the performance of polymer solar cells even in the absence of increase in light absorption. The improvement in electronic performance of the devices could be attributed to the hole blocking properties of ZnO layer in combination with a reduction of contact resistance and charge recombination at the polymer blend/Al interface. More importantly, we could show for the first time that the morphology of OSP is a crucial parameter to obtain highly efficient solar cells in normal device structures. Cluster free ZnO nanoparticle solution could be prepared by ethanolamine surface modification that allowed the processing of ZnO OSP with improved layer morphology nanoparticle as well as improved contact resistance compared to untreated ZnO. By optimizing optical, morphological and electronic properties of ZnO based OSP layers, we obtain PTB7:$PC_{70}BM$ solar cells with 7.6%, using normal device with all solution processed interlayers. To further increase the efficiency in PTB7 solar cells using normal device structures,

combining ethanolamine modified ZnO OSP layers with thicker PTB7:$PC_{70}BM$ layers is a promising approach.

4. Experimental Section

ZnO Synthesis and IPA Solutions: ZnO nanoparticles were prepared as published elsewhere.[26] A solution of 0.4415 g of potassium hydroxide KOH (Aldrich Chemicals 99.99%) in 23 mL of methanol was added dropwise to a solution of 0.8202 g of zinc acetate $Zn(Ac)_2$ (Aldrich Chemicals 99.99%) in 42 mL of methanol (Acros 99.99%) and 0.25 mL of distilled water at 60 °C under magnetic stirring (mole ratio KOH/$Zn(Ac)_2$ = 1.54). After 2 h 15 min, the mixture was concentrated by using a rotary pump. Then, the solution was left at rest to decant and the white solid precipitate was washed with methanol. ZnO nanoparticles with 6 nm as average diameter were formed as shown in Figure 1a. The solution-processable n-type semiconductor inks were prepared by transferring the as synthesized ZnO nanoparticles from methanol to isopropanol (IPA) mixed with ethanolamine (0.2 wt%) (EA).[26] The amount of EA used was optimized so that isolated nanoparticles were obtained in IPA and the solar cell performance was optimal. Indeed, high amount of EA introduce isolating barrier between nanoparticles that reduce the electric performance of the interfacial layer, as also observed inverted solar cells.[11] It was observed that grafting of EA to ZnO at optimal concentration of 0.2 wt% only slightly decreased the conductivity of the interfacial layers. After mixing of EA and ZnO in IPA, small optical changes of the ZnO solution are visible already seconds after the introduction of EA due to the spontaneous grafting of EA on the surface of ZnO. However, ultrasonic treatment was applied for 30 min, during which solubility of the ZnO nanoparticle was gradually increased until isolated nanoparticles were obtained in IPA. By this technique, cluster free ZnO nanosphere solution in isopropanol of concentrations of 2, 5, 7.5, 10 and 20 mg mL^{-1} could be obtained.

Nanoparticle Characterization: Size and shape of ZnO nanoparticles were characterized by high-resolution transmission electron microscopy (HR-TEM) (JEOL 3010, acceleration voltage of 300 kV). The samples were prepared by drop-casting a ZnO IPA solution onto a carbon-coated copper grid. The size of aggregates of ZnO nanoparticle in isopropanol before and after EA modification was determined by differential light scattering using a Malvern Zetasizer. UV–Vis absorption and fluorescence investigations of the ZnO nanoparticles in solution were recorded using a Varian CARY 5000 spectrophotometer and a CARY Eclipse spectrometer, respectively. The surface morphology of ZnO nanoparticle layers deposited on top of P3HT:PCBM layers was studied by atomic force microscopy (AFM) using a Nanoscope III in taping mode. Ultraviolet photoelectron spectroscopy (UPS) and X-ray photoelectron spectroscopy (XPS) measurements were performed in an ultrahigh vacuum (UHV) surface analysis system with a Scienta-200 hemispherical analyzer by using ZnO nanoparticle samples spin-coated onto ITO substrates with the resulting film thickness ≈20 nm. UPS and XPS measurement were calibrated by referencing to Fermi level and Au $4f_{7/2}$ peak position of the Ar+ ion sputter-clean gold foil. UPS was carried out with an unfiltered HeI ($h\nu$ = 21.22 eV) to characterize the vacuum level and the valance states with an error margin of ±0.05 eV. The work function was derived from the secondary electron cut-off. XPS was measured with a monochromatized Al $K\alpha$ source ($h\nu$ = 1486.6 eV).

Solar Cell Fabrication and Characterizaton: Solar cells in normal device structure were processed as follow. First ITO substrates (purchased from OSILLA and LUMTEC) were thoroughly cleaned by sonication in acetone and ethanol followed by rinsing with water and sonication in isopropanol and applying ultraviolet-ozone for 10 min. A thin layer of poly(3,4-PEDOT:PSS) (CLEVIOSTM AI 4083) was spin-coated on the cleaned ITO pre-coated glass substrate at the speed of 4000 rpm for 60 s followed by heating on a hot-plate at 140 °C for 15 min. The substrates were then transferred to a nitrogen-filled glove box. P3HT and $PC_{60}BM$ were purchased from Sigma-Aldrich and Solenne (purity 95%), respectively. P3HT:$PC_{60}BM$ blends with a weight ratio of 1:1 using 25 mg mL^{-1} P3HT were dissolved in a chlorobenzene/1,8-octanedithiol (97:3 vol%) solvent mixture and then spin-coated at the speed of 1500 rpm for 60 s. The blend layers were aged for 20 min and annealed for 15 min at 150 °C. Alternatively, we used a drying step of the active layer in vacuum without thermal annealing. Here the active layers were transferred into high vacuum for 12 h instead of annealing. Interlayers of ZnO nanoparticles were processed by spin-coating ZnO inks with different concentrations from 2 mg mL^{-1} to 20 mg mL^{-1} on top of the active layers at 1500 rpm for 60 s followed by annealing for 5 min at 80 °C, all processes were done inside the glove box.

PTB7 (1-Material) and $PC_{70}BM$ (Solenne, purity 95%) were solubilized over night in mixed solvents of chlorobenzene/1,8-diiodoctane (97:3% by volume) with a weight ratio of 1:1.5 using 10 mg mL^{-1} PTB7. The PTB7:$PC_{70}BM$ blend layer, with a nominal thickness of 90 nm, was prepared by spin-coating at 1800 rpm for 2 min. After dried in vacuum over night, different concentration of ZnO nanoparticles in isopropanol and 0.2% (v/v) ethanol amine was spin-coated on the top of active layers at 1500 rpm for 1 min and dried at hot plate at 80 °C for 5 min. In order to study the impact of ZnO layers in detail, we prepared sets of devices under identical conditions by only changing one parameter such as for example ZnO concentration in IPA.

For processing the cathode, samples were put into a MBRAUN evaporator inside the glovebox, in which Al metal electrodes (100 nm) were thermally evaporated at 2×10^{-6} Torr pressure through a shadow mask and the device area was 0.055 cm^2 and 0.24 cm^2 for Ossila and Lumtec substrates, respectively. The current density–voltage (J–V) characteristics of the devices were measured using a Keithley 238 Source Measure Unit inside the glove box using Lumtec substrates. Solar cell performance was measured by using a Newport class AAA 1.5 Global solar simulator (Oriel Sol3ATM model n° 94043A) with an irradiation intensity of 100 mW cm^{-2}. The light intensity was determined with a Si reference cell (Newport Company, Oriel n° 94043A) calibrated by National Renewable Energy Laboratory (NREL). Spectral mismatch factors (M) were calculated according to a standard procedure,[42] and M values of 1.02 and 1.03 were obtained for the PTB7:PCBM and P3HT:PCBM devices, respectively. These values were used to correct the measured I_{sc} values of the solar cells to I_{sc} values corresponding to AM1.5G conditions. Shadow masks were used to well-define the illuminated area to 0.24 × 1.0 cm^2. Comparison of masked and unmasked solar cells gave consistent results with photocurrent increase by less 2% for unmasked devices. Performance of the best devices was presented, while average PCEs were obtained with standard deviation analysis calculated using nine devices and are shown in the Table 1 and S1 (Supporting Information).

External quantum efficiency (EQE) measurements were performed in air using a homemade setup consisting of a Keithley 238 Source Measure Unit and Newport monochromator. Light intensity was measured with a calibrated Si-diode from Newport Company.

Optical Simulations of the Solar Cells: First ellipsometric measurements were performed on all layers of the solar cell using a rotating-polarizer ellipsometer (Semilab GES5) on layers coated on Si substrates as the refractive index difference between the silicon substrate and the organic films is high enough to ensure high reflection coefficients at the organic/Si interface.[32] SEA software (Semilab company) was used to fit the SE measurements of $\tan(\Psi)$ and $\cos(\Delta)$ and extract the optical indices $n(\lambda)$ and $k(\lambda)$ of the materials.[32] The spectrophotometric measurements of each layer were realized with a CARY 5000 spectrophotometer from Varian equipped with an integrating sphere. Layer thicknesses were determined with a mechanical profilometer in combination by AFM cross section measurements (more details in the Supporting Information).

Electronic Characterization of the ZnO Interfaces Inside the Solar Cells: Impedance spectroscopy measurements were performed using an Autolab PGSTAT-30 equipped with a frequency analyzer module. A small voltage perturbation (20 mV rms) is applied at frequencies from 1 MHz to 1 Hz. Measurements were carried out under 1 sun light intensity calibrated with a monocrystalline silicon photodiode sweeping the DC voltage in the range 0 to V_{oc}. Recombination resistance (R_{rec}) and chemical capacitance (C_μ) are directly extracted from the high-frequency region as previously reported [43] and the contact resistance

under low frequencies. A complete analysis will be published elsewhere. The transient open circuit voltage decay (TOCVD) methodology used in the present study has been reported by Thakur et al.[36,37] The solar cells were illuminated by driving the LED with square wave pulses. The LED input and solar cell output were synchronized and recorded in a 4-channel digital oscilloscope from Agilent Technology.

Supporting Information

Supporting Information is available from the Wiley Online Library or from the author.

Acknowledgements

The authors acknowledge financial support by the French *Fond Unique Intermistériel* (FUI) under the project "SFUMATO" (Grant number: F1110019V/201308815) as well as by the European Commission under the Project "SUNFLOWER" (FP7), grant agreement number 287594. Generalitat Valenciana (ISIC/2012/008 Institute of Nanotechnologies for Clean Energies) is also acknowledged for providing financial support.

Received: May 14, 2014
Revised: June 12, 2014
Published online:

[1] J. You, L. Dou, K. Yoshimura, T. Kato, K. Ohya, T. Moriarty, K. Emery, C.-C. Chen, J. Gao, G. Li, Y. Yang, *Nat. Commun.* **2013**, *4*, 1446.
[2] W. Li, K. H. Hendriks, W. S. C. Roelofs, Y. Kim, M. M. Wienk, R. A. J. Janssen, *Adv. Mater.* **2013**, *25*, 3182.
[3] L.-M. Chen, Z. Xu, Z. Hong, Y. Yang, J. Mater, *Chem.* **2010**, *20*, 2575.
[4] R. Po, C. Carbonera, A. Bernardi, N. Camaioni, *Energy Environ. Sci.* **2011**, *4*, 285.
[5] S. Shao, K. Zheng, T. Pullerits, F. Zhang, *ACS Appl. Mater. Interfaces* **2013**, *5*, 380.
[6] P. P. Boix, J. Ajuria, I. Etxebarria, R. Pacios, G. Garcia-Belmonte, J. Bisquert, *J. Phys. Chem. Lett.* **2011**, *2*, 407.
[7] S. Wilken, D. Scheunemann, V. Wilkens, J. Parisi, H. Borchert, *Org. Electron.* **2012**, *13*, 2386.
[8] S. K. Hau, H.-L. Yip, N. S. Baek, J. Zou, K. O'Malley, A. K.-Y. Jen, *Appl. Phys. Lett.* **2008**, *92*, 253301.
[9] Z. Liang, Q. Zhang, O. Wiranwetchayan, J. Xi, Z. Yang, K. Park, C. Li, G. Cao, *Adv. Funct. Mater.* **2012**, *22*, 2194.
[10] M. J. Tan, S. Zhong, J. Li, Z. Chen, W. Chen, *ACS Appl. Mater. Interfaces* **2013**, *5*, 4696.
[11] B. R. Lee, E. D. Jung, Y. S. Nam, M. Jung, J. S. Park, S. Lee, H. Choi, S.-J. Ko, N. R. Shin, Y.-K. Kim, S. O. Kim, J. Y. Kim, H.-J. Shin, S. Cho, M. H. Song, *Adv. Mater.* **2014**, *26*, 494.
[12] A. Hayakawa, O. Yoshikawa, T. Fujieda, K. Uehara, S. Yoshikawa, *Appl. Phys. Lett.* **2007**, *90*, 163517.
[13] J. You, C.-C. Chen, L. Dou, S. Murase, H.-S. Duan, S. A. Hawks, T. Xu, H. J. Son, L. Yu, G. Li, Y. Yang, *Adv. Mater.* **2012**, *24*, 5267.
[14] R. Steim, S. A. Choulis, P. Schilinsky, C. J. Brabec, *Appl. Phys. Lett.* **2008**, *92*, 093303.
[15] K. D. G. I. Jayawardena, R. Rhodes, K. K. Gandhi, M. R. R. Prabhath, G. D. M. R. Dabera, M. J. Beliatis, L. J. Rozanski, S. J. Henley, S. R. P. Silva, *J. Mater. Chem. A* **2013**, *1*, 9922.
[16] H. Ma, H. L. Yip, F. Huang, A. K. Y. Jen, *Adv. Funct. Mater.* **2010**, *20*, 1371.
[17] J. Gilot, I. Barbu, M. M. Wienk, R. A. J. Janssen, *Appl. Phys. Lett.* **2007**, *91*, 113520.
[18] A. Roy, S. H. Park, S. Cowan, M. H. Tong, S. Cho, K. Lee, A. J. Heeger, *Appl. Phys. Lett.* **2009**, *95*, 013302.
[19] B. Jin, Y. Kim, S. H. Kim, H. Lee, K. Lee, W. Ma, X. Gong, A. J. Heeger, *Adv. Mater.* **2006**, *18*, 572.
[20] P. D. Andersen, J. C. Skårhøj, J. W. Andreasen, F. C. Krebs, *Opt. Mater.* **2009**, *31*, 1007.
[21] A. K. K. Kyaw, D. H. Wang, D. Wynands, J. Zhang, T.-Q. Nguyen, G. C. Bazan, A. J. Heeger, *Nano Lett.* **2013**, *13*, 3796.
[22] B. A. Collins, Z. Li, J. R. Tumbleston, E. Gann, C. R. Mcneill, H. Ade, *Adv. Energy Mater.* **2012**, *3*, 65.
[23] Z. He, C. Zhong, S. Su, M. Xu, H. Wu, Y. Cao, *Nat. Photonics* **2012**, *6*, 591.
[24] A. Guerrero, N. F. Montcada, J. Ajuria, I. Etxebarria, R. Pacios, G. Garcia-Belmonte, E. Palomares, *J. Mater. Chem. A* **2013**, *1*, 12345.
[25] C. Waldauf, M. Morana, P. Denk, P. Schilinsky, K. Coakley, S. A. Choulis, C. J. Brabec, *J. Appl. Phys. Lett.* **2006**, *89*, 233517.
[26] A. K. Diallo, M. Gaceur, N. Berton, O. Margeat, J. Ackermann, C. Videlot-Ackermann, *Superlattices Microstruct.* **2013**, *58*, 144.
[27] S. Shao, K. Zheng, T. Pullerits, F. Zhang, *ACS Appl. Mater. Interfaces* **2013**, *5*, 380.
[28] Q. Bao, X. Liu, S. Braun, M. Fahlman, *Adv. Energy Mater.* **2014**, DOI: 10.1002/aenm.201301272.
[29] H. Aarnio, P. Sehati, S. Braun, M. Nyman, M. P. de Jong, M. Fahlman, R. Österbacka, *Adv. Energy Mater.* **2011**, *1*, 792.
[30] R. J. Davis, M. T. Lloyd, S. R. Ferreira, M. J. Bruzek, S. E. Watkins, L. Lindell, P. Sehati, M. Fahlman, J. E. Anthony, J. W. P. Hsu, *J. Mater. Chem.* **2011**, *21*, 1721.
[31] L. A. A. Pettersson, L. S. Roman, O. Inganäs, *J. Appl. Phys.* **1999**, *86*, 487–496.
[32] D. Duché, F. Bencheikh, S. Ben Dkhil, M. Gaceur, N. Berton, O. Margeat, J. Ackermann, J.-J. Simon, L. Escoubas, *Sol. Energy Mater. Sol. Cells* **2014**, *126*, 197–204.
[33] A. Guerrero, S. Loser, G. Garcia-Belmonte, C. J. Bruns, J. Smith, H. Miyauchi, S. I. Stupp, J. Bisquert, T. J. Marks, *Phys. Chem. Chem. Phys.* **2013**, *15*, 16456.
[34] A. Guerrero, T. Ripolles-Sanchis, P. P. Boix, G. Garcia-Belmonte, *Org. Electron.* **2012**, *13*, 2326.
[35] P. P. Boix, A. Guerrero, L. F. Marchesi, G. Garcia-Belmonte, J. Bisquert, *Adv. Energy Mater.* **2011**, *1*, 1073.
[36] A. K. Thakur, H. Baboz, G. Wantz, J. Hodgkiss, L. Hirsch, *J. Appl. Phys.* **2012**, *112*.
[37] A. K. Thakur, G. Wantz, G. Garcia-Belmonte, J. Bisquert, L. Hirsch, *Sol. Energy Mater. Sol. Cells* **2011**, *95*, 2131.
[38] G. Mattioli, S. Ben Dkhil, M. I. Saba, G. Malloci, C. Melis, P. Alippi, F. Filippone, P. Giannozzi, A. K. Thakur, M. Gaceur, O. Margeat, A. K. Diallo, C. Videlot-Ackermann, J. Ackermann, A. A. Bonapasta, A. Mattoni, *Adv. Energy Mater.* **2014**, DOI: 10.1002/aenm.201301694.
[39] T. Kirchartz, B. E. Pieters, J. Kirkpatrick, U. Rau, Jenny Nelson, *Phys. Rev. B* **2011**, *83*, 115209.
[40] M. Al-ibrahim, O. Ambacher, S. Sensfuss, G. Gobsch, *Appl. Phys. Lett.* **2005**, *86*, 201120.
[41] B. G. Li, Y. Yao, H. Yang, V. Shrotriya, G. Yang, Y. Yang, *Adv. Funct. Mater.* **2007**, *17*, 1636.
[42] V. Shrotriya, G. Li, Y. Yao, T. Moriarty, K. Emery, Y. Yang, *Adv. Funct. Mater.* **2006**, *16*, 2016.
[43] G. Garcia-Belmonte, A. Guerrero, J. Bisquert, *J. Phys. Chem. Lett.* **2013**, *4*, 877.
[44] S. Foster, F. Deledalle, A. Mitani, T. Kimura, K.-B. Kim, T. Okachi, T. Kirchartz, J. Oguma, K. Miyake, J. R. Durrant, S. Doi, J. Nelson, *Adv. Energy Mater.* **2014**, DOI: 10.1002/aenm.201400311.